



Binding Energy of ^{79}Cu : Probing the Structure of the Doubly Magic ^{78}Ni from Only One Proton Away

A. Welker,^{1,2,*} N. A. S. Althubiti,³ D. Atanasov,^{4,†} K. Blaum,⁴ T. E. Cocolios,⁵ F. Herfurth,⁶ S. Kreim,^{4,‡}
 D. Lunney,⁷ V. Manea,^{2,4} M. Mougeot,⁷ D. Neidherr,⁶ F. Nowacki,^{8,9} A. Poves,^{10,11} M. Rosenbusch,^{12,§}
 L. Schweikhard,¹² F. Wienholtz,^{2,12} R. N. Wolf,^{4,¶} and K. Zuber¹

¹*Technische Universität Dresden, 01069 Dresden, Germany*

²*CERN Geneva, 1211 Geneva, Switzerland*

³*University of Manchester, Manchester M13 9PL, United Kingdom*

⁴*Max-Planck-Institut für Kernphysik, 69117 Heidelberg, Germany*

⁵*KU Leuven, Instituut voor Kern- en Stralingsfysica, 3001 Leuven, Belgium*

⁶*GSI Helmholtzzentrum für Schwerionenforschung GmbH, 64291 Darmstadt, Germany*

⁷*CSNSM-IN2P3-CNRS, Université Paris-Sud, 91405 Orsay, France*

⁸*Université de Strasbourg, IPHC, 67037 Strasbourg, France*

⁹*CNRS, UMR7178, 67037 Strasbourg, France*

¹⁰*Departamento de Física Teórica and IFT-UAM/CSIC, Universidad Autónoma de Madrid, E-28049 Madrid, Spain*

¹¹*Institute for Advanced Study, Université de Strasbourg, 67083 Strasbourg, France*

¹²*Ernst-Moritz-Arndt-Universität, Institut für Physik, 17487 Greifswald, Germany*

(Received 9 June 2017; revised manuscript received 31 July 2017; published 6 November 2017)

The masses of the neutron-rich copper isotopes $^{75-79}\text{Cu}$ are determined using the precision mass spectrometer ISOLTRAP at the CERN-ISOLDE facility. The trend from the new data differs significantly from that of previous results, offering a first accurate view of the mass surface adjacent to the $Z = 28$, $N = 50$ nuclide ^{78}Ni and supporting a doubly magic character. The new masses compare very well with large-scale shell-model calculations that predict shape coexistence in a doubly magic ^{78}Ni and a new island of inversion for $Z < 28$. A coherent picture of this important exotic region begins to emerge where excitations across $Z = 28$ and $N = 50$ form a delicate equilibrium with a spherical mean field.

DOI: [10.1103/PhysRevLett.119.192502](https://doi.org/10.1103/PhysRevLett.119.192502)

The $Z = 28$, $N = 50$ region of the nuclear chart is a focus of today's experimental and theoretical nuclear-structure research with the nuclide ^{78}Ni representing a frontier. Over the years experiments with radioactive-ion beams have shown that the stability of nuclear magic numbers breaks down in light, exotic nuclei as reviewed in Ref. [1]. The stakes for ^{78}Ni are double, as it lies at the intersection of the classical proton and neutron shell closures $Z = 28$ and $N = 50$, respectively. Whether the exotic ^{78}Ni retains the exceptional stability of the classic closed-shell nuclides is an open question, upon which depends the correct description of medium-mass, neutron-rich nuclei.

Crucial for developing more reliable solutions to the nuclear many-body problem is the understanding of the mechanism driving shell evolution in exotic nuclei. In the shell model, the tensor force has been proposed as a fundamental ingredient [2]. With the advances in effective

field theory and in-medium similarity renormalization group methods [3], shell-closure signatures become important links between shell-model and *ab initio* approaches, as recently illustrated for the purported magic numbers $N = 32$ [4–6] and $N = 34$ [7]. This complementarity was recently highlighted with the structure of ^{78}Ni described using two such approaches: a large-scale shell-model calculation [8] and a coupled-cluster calculation using a chiral Hamiltonian [9]. The two calculations agree on the excitation energy of the first 2^+ state, suggesting doubly magic character. However, the shell-model calculations also predict an intruder 0_2^+ state at a lower excitation energy than the 2^+ state, hinting at a new (fifth) island of inversion following those at $N = 8, 20, 28$, and 40 [8]. While these predictions cannot yet be tested directly with the concerned $N = 50$ isotones, the copper isotopes in the vicinity of ^{78}Ni provide an excellent proxy, as the ensemble of ground-state properties and spectroscopy is very sensitive to the two-body matrix elements promoting protons across $Z = 28$ and neutrons across $N = 50$. Blocking cross-shell excitations above $Z = 28$ inaccurately described the $1/2^-$ state systematics and the $^{71,73}\text{Cu}$ magnetic moments [10,11], whereas allowing proton excitations from the $f_{7/2}$ level gave a good description of the evolution of the $1/2^-$ state with N [12]. Similar conclusions resulted

Published by the American Physical Society under the terms of the Creative Commons Attribution 4.0 International license. Further distribution of this work must maintain attribution to the author(s) and the published article's title, journal citation, and DOI.

from the Coulomb-excitation study of the neighboring zinc isotopes: with an inert ^{56}Ni core a very large proton effective charge was necessary to correctly reproduce the experimental quadrupole transition probabilities, suggesting important proton-core polarization [13].

Ground-state properties provide complementary information. For example, recent β -decay half-lives [14] show a sudden drop crossing the nickel chain at $N = 50$, consistent with ^{78}Ni being doubly magic. Very recent studies by laser spectroscopy offer strong evidence for shape coexistence close to ^{78}Ni [15]. The magnetic moment and the charge radius of the $1/2^+$ isomer in ^{79}Zn suggest an intrinsically deformed structure dominated by multiparticle-multihole excitations across $N = 50$ [15,16]. On the other hand, a 0_2^+ intruder state at even lower excitation energy (639 keV) was proposed for ^{80}Ge , suggesting the possibility of an intruder 0_2^+ state in ^{78}Ni [17]. Binding energies, obtained via mass measurements, bring decisive information since any nuclide's configuration minimizes the ground-state energy.

In this Letter we report high-precision masses of the $Z = 29$ copper isotopes $^{75-79}\text{Cu}$, determined by a combination of sensitive mass-spectrometry techniques by the ISOLTRAP experiment [18–20] and high production by the ISOLDE facility at CERN [21]. The new masses are between 5 and 100 times more precise than previous values, obtained via a deflecting magnetic dipole at the Holifield Radioactive Ion Beam Facility [22]. They establish for the first time the trend of neutron separation energies up to $N = 50$, only one proton away from ^{78}Ni .

The $^{75-79}\text{Cu}$ isotopes were produced using a uranium target induced to fission using spallation neutrons created from a tungsten converter, a technique that suppresses neutron-deficient isobaric contaminations [23], combined with resonant laser ionization [24]. The ion beam was accelerated to an energy of 30 keV and transported through the ISOLDE high-resolution mass separator. The copper ions of interest and the isobaric contaminants (primarily gallium and rubidium, the yields of which were between 10^2 and 10^4 times more abundant) were accumulated in ISOLTRAP's helium-gas-filled linear radio-frequency quadrupole [25] for 10 ms.

The ion bunch was then injected into the multireflection time-of-flight (MR-TOF) mass separator (MS) [26,27] where, after multiple revolutions between its electrostatic mirrors, the separated isobars were detected by use of an electron multiplier. The relationship between the mean time of flight t of an ion species (between the ISOLTRAP buncher and the detector) and its mass-to-charge ratio m/q is given by $t = \alpha(m/q)^{1/2} + \beta$, where α and β are calibration constants. The obtained time-of-flight spectrum was calibrated using the gallium isobars and $^{85}\text{Rb}^+$ ions from an off-line ion source. The formula linking the mass of the ion of interest to the masses of the reference ions is [4]

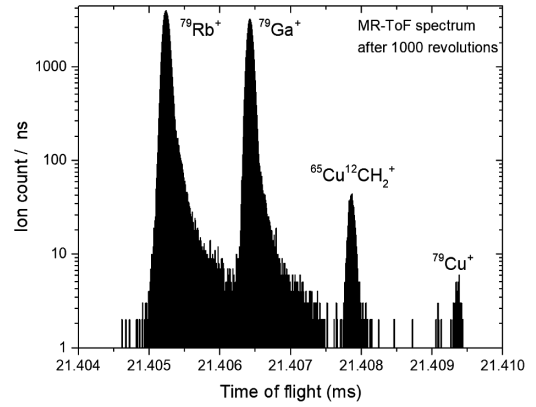


FIG. 1. MR-TOF spectrum of $^{79}\text{Cu}^+$ and isobaric species after 1000 revolutions. For details see the text.

$$\sqrt{m} = C_{\text{TOF}}(\sqrt{m_1} - \sqrt{m_2}) + 1/2(\sqrt{m_1} + \sqrt{m_2}), \quad (1)$$

where $C_{\text{TOF}} = (2t - t_1 - t_2)/[2(t_1 - t_2)]$ is the experimental time-of-flight ratio of the ion of interest and the reference ions. A representative time-of-flight spectrum used to determine the mass of ^{79}Cu is shown in Fig. 1.

For the Penning-trap mass measurements, the time and duration of the MR-TOF MS ejection pulse, acting on the in-trap lift cavity, was chosen to ensure that lighter contaminants are not in the cavity when it is switched to ejection potential and that heavier contaminants are still in the cavity when it is switched back to trapping potential [28]. Thus, ions in front of and behind the ions of interest are not transferred to the Penning traps. The purified copper-ion ensemble was then cooled and recentered for 80 ms in the helium buffer-gas-filled preparation Penning trap and subsequently injected in the precision Penning trap, where high-precision mass measurements were carried out by time-of-flight ion-cyclotron resonance [29]. Three such resonances were recorded for $^{75}\text{Cu}^+$, three for $^{76}\text{Cu}^+$, four for $^{77}\text{Cu}^+$, and one for $^{78}\text{Cu}^+$, which is shown in Fig. 2. No statistically significant amount of the isomeric state proposed in Ref. [30] was observed in the $^{76}\text{Cu}^+$ data.

The cyclotron-frequency ratio between the reference $^{85}\text{Rb}^+$ ions and the copper ions of interest, $r = \nu_{c,\text{ref}}/\nu_c$ was measured, leading to the atomic mass M as $M = r(M_{\text{ref}} - m_e) + m_e$, where m_e is the electron mass and M_{ref} is the mass of the reference nuclide. The use of the MR-TOF MS allowed measuring at a lower yield than would have been possible solely by Penning-trap mass spectrometry. Some 300 ^{79}Cu ion events were collected, corresponding to a yield of only about 2 ions/ μC . The results of the measurement campaign are summarized in Table I. The mass excess of ^{77}Cu resulting from the MR-TOF measurement is $\text{ME}(^{77}\text{Cu}) = -48\,876(9)$ keV, in reasonable agreement with the Penning-trap result, indicating the systematic error of the device. In Fig. 3(a) we present the two-neutron separation energies

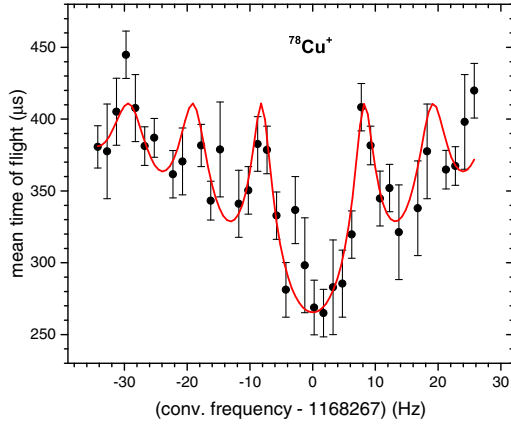


FIG. 2. The time-of-flight ion-cyclotron resonance with an excitation time of $T_{\text{ex}} = 100$ ms of $^{78}\text{Cu}^+$. The solid line is a fit of the data to the theoretical line shape [29].

$S_{2n} = -\text{ME}(N, Z) + \text{ME}(N - 2, Z) + 2\text{ME}_n$ of the nuclides in the ^{78}Ni region. Here, $\text{ME}(N, Z)$ represents the nuclide mass excess and ME_n is the neutron mass excess. One notices very clearly the drop in S_{2n} at the crossing of $N = 50$ for $Z = 30$, which is in most cases a well-known sign for magicity. The new trend differs significantly from the one based on measurements performed at the Holifield facility [22], shown in Fig. 3(b). However, the large uncertainties made it rather difficult to establish a clear signature. The trend of the S_{2n} values based on the new measurements is linear up to $N = 50$. The new masses do not extend beyond $N = 50$, so it is not possible to observe the expected S_{2n} drop between $N = 50$ and $N = 52$. However, the effect of the magic number is already noticeable in the S_{2n} difference between $N = 48$ and $N = 50$ (we return to this point later).

The nuclear shell model can explain the binding of $Z = 28$ and $N = 50$ shells towards ^{79}Cu . To this end, we performed large-scale shell-model calculations in a model space that incorporates the degrees of freedom needed for the mass description in the range $40 \leq N \leq 52$. In the

following we employ the recently developed PFS DG-U interaction [8]. This interaction spans a model space comprising $f_{7/2}, p_{3/2}, f_{5/2}, p_{1/2}$ orbitals for protons and $g_{9/2}, d_{5/2}, s_{1/2}, g_{7/2}, d_{3/2}$ orbitals for neutrons and has the advantage of incorporating both $g_{9/2} - g_{7/2}$ and $d_{5/2} - d_{3/2}$ neutron spin-orbit partners. The configurational valence space is extended up to eight particle-hole excitations across the $Z = 28$ and the $N = 50$ gaps and ensures convergence of the wave functions.

The S_{2n} values calculated with the new PFS DG-U interaction are compared with the experimental results for Cu and the neighboring Ni and Zn chains [Fig. 3(a)]. The agreement between the calculation and the experimental results is excellent for Ni and Cu isotopes and gives confidence in the underlying shell-model description of these exotic nuclides. The underbinding of the $N = 44$ -46 Zn isotopes results from not mixing the neutron orbitals between the pf and sdg valence spaces. For these nuclides the experimental ground-state spin appears to be of non-natural parity and can only be generated by allowing such neutron core excitations, which are known to be of increasing importance for neutron-deficient $N = 40$ isotones [33].

To highlight the decisive improvement brought by the new interaction, we also compare the results of a calculation with the JUN45 interaction [34], for which the two-body matrix elements are optimized to describe the properties of nuclei in a valence space with closed $Z = 28$ and $N = 50$ cores [Fig. 3(b)]. The S_{2n} trends differ significantly with the choice of interaction and model space. In particular, the S_{2n} values are overbound between $N = 46$ and $N = 50$ for calculations with the restricted JUN45 configuration compared to the PFS DG-U result, while the S_{2n} values up to $N = 46$ are described by both interactions. The necessity of masses measured with high accuracy, as well as high precision, is clearly illustrated and the present results indicate the success of the new calculations over the ones with no $Z = 28$ and/or $N = 50$ core excitations.

TABLE I. Frequency ratios $r = \nu_{c,\text{ref}}/\nu_c$, time-of-flight ratios C_{TOF} , and resulting mass excesses of the copper isotopes measured in this work. Mass-excess values from Atomic Mass Evaluation 2016 (AME2016) [31] are also given (the # sign indicates extrapolated values—note that the authors of AME2016 considered these extrapolations to be more reliable than the measured values of Ref. [22]). Reference-mass values are from Ref. [31]. The statistical and the systematic uncertainties of the measurements are combined in quadrature in the value displayed between the parentheses. Experimental half-lives are taken from Ref. [32]. The yield values are estimated from the approximate 3% ISOLTRAP efficiency for the MR-TOF MS.

| A | Yield (Ions/ μC) | Half-life (ms) | Reference ion | Ratio r or C_{TOF} | Mass Excess (keV) | |
|----|------------------------------|----------------|--------------------------------------|-------------------------------------|-------------------|--|
| | | | | | This work | AME2016 |
| 75 | 1.5×10^4 | 1224 (3) | $^{85}\text{Rb}^+$ | $r = 0.8825801431$ (95) | -54 470.04 (76) | -54 471.3 (2.3) |
| 76 | 4×10^2 | 637.7 (5.5) | $^{85}\text{Rb}^+$ | $r = 0.8944012520$ (115) | -50 981.55 (89) | -50 976 (7) |
| 77 | 1×10^2 | 467.9 (2.1) | $^{85}\text{Rb}^+$ | $r = 0.9062050439$ (150) | -48 862.8 (1.2) | -48 620 [#] (150 [#]) |
| 78 | 1×10^1 | 330.7 (2.0) | $^{85}\text{Rb}^+$ | $r = 0.918033767$ (213) | -44 772 (17) | -44 500 (500) |
| | | | $^{78}\text{Ga}^+, ^{85}\text{Rb}^+$ | $C_{\text{TOF}} = 0.49703172$ (352) | -44 819 (22) | |
| 79 | 2 | 241.0 (3.2) | $^{79}\text{Ga}^+, ^{85}\text{Rb}^+$ | $C_{\text{TOF}} = 0.4963169$ (192) | -42 408 (105) | -41 740 [#] (300 [#]) |

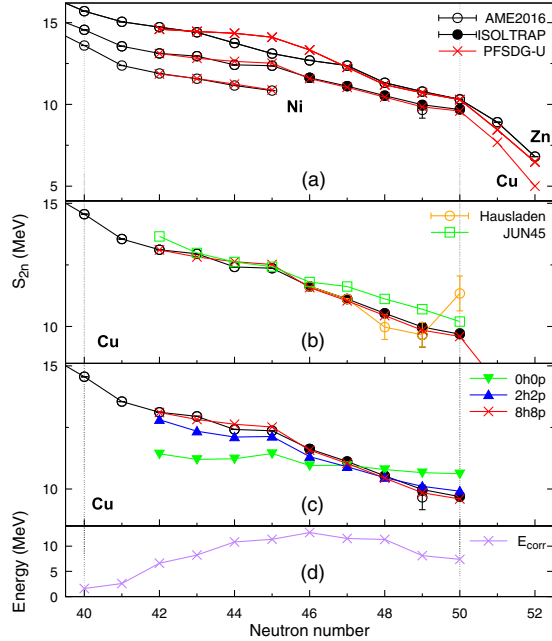


FIG. 3. (a) Experimental two-neutron separation energies along the nickel, copper, and zinc chains compared to large-scale shell-model calculations using the PFSDG-U interaction (crosses). The experimental data are from Atomic Mass Evaluation 2016 (AME2016) [31] (open circles) and ISOLTRAP (full black circles). (b) Comparison of S_{2n} values calculated with the PFSDG-U and JUN45 (open green squares) interactions with the present experimental data, and AME2016 and previous results [22] (open orange circles). (c) Evolution of the calculated S_{2n} values in the copper chain as a function of the number of particle-hole excitations across the $Z = 28$ and $N = 50$ gaps. (d) PFSDG-U correlation energies for the $^{69-79}\text{Cu}$ isotopes.

To understand the differences observed in Fig. 3(b) between the two calculations, we represent the evolution of the calculated S_{2n} as a function of the number of particle-hole excitations across the $Z = 28$ and $N = 50$ shell gaps [Fig. 3(c)]. There is a clear asymmetry in the correlation mechanism between $N \leq 47$ and $N \geq 47$ essentially reflecting two features: the neutron shell closures at $N = 40$ and $N = 50$, as well as the associated particle-hole conjugation. The correlations describe an inverse parabolic behavior whose derivative should vanish at midshell $N = 45$ and change sign as seen in Fig. 3(d). In addition, the effective single particle energies reveal a simultaneous proton and neutron gap reduction towards $Z = 28$ and $N = 50$, which slightly shifts the maximum correlation energy point to $N = 46$. This evolution of the correlation energy is well reflected in the S_{2n} trend, which is more flat before $N = 45$, and more abrupt afterwards.

The strong sensitivity of the correlations to ^{78}Ni -core excitations is intimately connected to the sizes of the proton and neutron gaps. From the effective single particle energies, the proton gap is considerably reduced from 6.7 MeV at $N = 40$ to 4.9 MeV at $N = 50$. This is

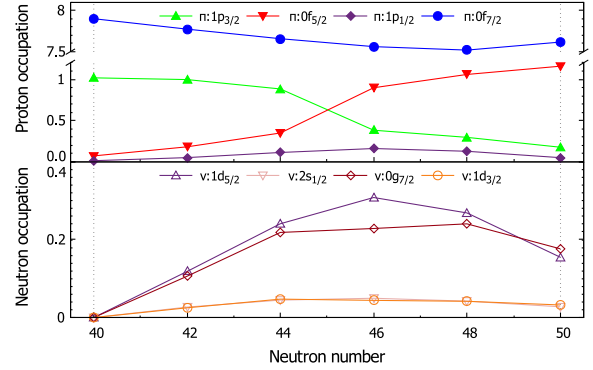


FIG. 4. Occupation levels from the PFSDG-U calculation given in total numbers of protons and neutrons along the copper chain (for even N).

essentially due to the strong $f_{5/2} - g_{9/2}$ proton-neutron attractive interaction whose main active components are spin orbit and tensor. This also causes the $f_{5/2}$ and $p_{3/2}$ orbitals to cross between $N = 44$ and $N = 46$ as reflected in the proton orbital occupancies plotted in Fig. 4.

One also notices the slight reduction of the $f_{7/2}$ orbital occupancy as a consequence of the proton gap reduction from ^{69}Cu ($N = 40$) towards ^{79}Cu ($N = 50$). The measured $f_{5/2} - p_{3/2}$ inversion [35] is perfectly accounted for by the new interaction, further reinforcing the confidence with which the nuclear structure of this important region can be described. Recent results from laser spectroscopy [36] also confirm the logic of this approach to correctly describe the g factors of $^{76,78}\text{Cu}$. Moreover, recent γ spectroscopy of proton knockout from ^{80}Zn [37] likewise points to a strong shell gap for ^{79}Cu .

Returning to the question of the $N = 50$ shell strength, in Fig. 5 we present the two-neutron shell gap

$$\Delta_{2n}(Z, N_0) = S_{2n}(Z, N_0) - S_{2n}(Z, N_0 + 2) \quad (2)$$

as a function of proton number, for the magic neutron numbers $N_0 = 28, 50, 82, 126$ in the upper curve. The lower curve shows the shell gap calculated using the isotope having two neutrons less than the magic number: $\Delta_{2n}(Z, N_0 - 2)$. The doubly magic nuclei show a local maximum of $\Delta_{2n}(Z, N_0)$ at the position of the proton magic number. Without exception, for each maximum in $\Delta_{2n}(Z, N_0)$ there is a minimum in $\Delta_{2n}(Z, N_0 - 2)$ at the same proton number Z . The overall behavior of $\Delta_{2n}(Z, N_0)$ was explained in Ref. [38] using a mean-field calculation, which showed that the peaked structure of the empirical shell gap is due to quadrupole correlations in the involved off-shell nuclides. The extent of quadrupole correlations in the $N_0 \pm 2$ isotopes depends strongly on Z , being minimal when crossing a magic number. The same argument applies for $\Delta_{2n}(Z, N_0 - 2)$. However, a local maximum for $\Delta_{2n}(Z, N_0)$

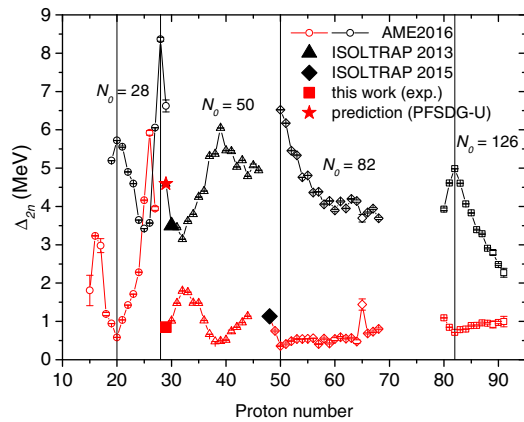


FIG. 5. Empirical two-neutron shell gap $\Delta_{2n}(Z, N_0)$ of neutron-magic nuclides (upper curves). The lower curves represent, for each magic neutron number N_0 , the shell gap computed for $\Delta_{2n}(Z, N_0 - 2)$. The data were taken from AME2016 [31] (open symbols), Refs. [39,40] (full black symbols), and this work (full red symbol). See the text, for details.

becomes a local minimum for $\Delta_{2n}(Z, N_0 - 2)$ because the binding energy of the neutron-magic nucleus appears in Eq. (2) with opposite sign. Observing $Z = 32$ (Ge) we note that the $N = 50$ two-neutron shell gap starts increasing towards $Z = 28$, while the $N_0 - 2$ values start decreasing. The present data allow computing the $N_0 - 2$ value, which shows a further decrease towards $Z = 28$, as expected for a doubly magic ${}^{78}\text{Ni}$. The new copper masses thus provide evidence for the doubly magic nature of ${}^{78}\text{Ni}$. The new shell-model results are nicely supported by the new measurements, giving confidence in the shell-gap prediction for N_0 , which is also shown in Fig. 5.

In conclusion, the masses of the neutron-rich isotopes ${}^{75-79}\text{Cu}$ were measured with a combination of Penning-trap and time-of-flight mass spectrometry, precisely defining the mass surface above ${}^{78}\text{Ni}$ and offering evidence for its doubly magic nature. Comparison of the new experimental two-neutron separation energies to large-scale shell-model calculations with the recently developed PFSDG-U interaction shows that excitations across $Z = 28$ and $N = 50$ are necessary in order to reproduce the new experimental trend, highlighting a delicate equilibrium between shape coexistence and a spherical mean field. The new data offer an important anchor point for calculations close to the doubly magic ${}^{78}\text{Ni}$, strengthening their extrapolations down $N = 50$ to a possible new island of inversion.

We thank the ISOLDE technical group and the ISOLDE Collaboration for support. We also acknowledge support by the BMBF (05P12HGCI1, 05P12HGFNE, and 05P15ODCIA), the Max Planck Society, French IN2P3, by the Alliance Program of the Helmholtz Association Contract No. HA216/EMMI, and the STFC under Grants No. ST/L005743/1 and No. ST/L005816/1. A. W.

acknowledges support by a Wolfgang Gentner Scholarship. This work is partly supported by MINECO (Spain) Grant No. FPA2014-57196, by the Program "Centros de Excelencia Severo Ochoa" SEV-2012-0249, and by a USIAS Fellowship at the Université de Strasbourg.

*Corresponding author.

andree.welker@cern.ch

†Present address: Technische Universität Dresden, 01069 Dresden, Germany.

‡Present address: Fakultät für Elektrotechnik, 68163 Mannheim, Germany.

§Present address: RIKEN Nishina Center for Accelerator-Based Science, 351-0198 Saitama, Japan.

¶Present address: ARC Centre of Excellence for Engineered Quantum Systems, The University of Sydney, NSW 2006, Australia.

- [1] O. Sorlin and M.-G. Porquet, *Prog. Part. Nucl. Phys.* **61**, 602 (2008).
- [2] T. Otsuka, T. Suzuki, R. Fujimoto, H. Grawe, and Y. Akaishi, *Phys. Rev. Lett.* **95**, 232502 (2005).
- [3] S. K. Bogner, H. Hergert, J. D. Holt, A. Schwenk, S. Binder, A. Calci, J. Langhammer, and R. Roth, *Phys. Rev. Lett.* **113**, 142501 (2014).
- [4] F. Wienholtz *et al.*, *Nature (London)* **498**, 346 (2013).
- [5] M. Rosenbusch *et al.*, *Phys. Rev. Lett.* **114**, 202501 (2015).
- [6] R. F. Garcia Ruiz *et al.*, *Nature Physics* **12**, 594 (2016).
- [7] D. Steppenbeck *et al.*, *Nature (London)* **502**, 207 (2013).
- [8] F. Nowacki, A. Poves, E. Caurier, and B. Bounthong, *Phys. Rev. Lett.* **117**, 272501 (2016).
- [9] G. Hagen, G. R. Jansen, and T. Papenbrock, *Phys. Rev. Lett.* **117**, 172501 (2016).
- [10] S. Franchou, M. Huyse, K. Kruglov, Y. Kudryavtsev, W. F. Mueller, R. Raabe, I. Reusen, P. Van Duppen, J. Van Roosbroeck, L. Vermeeren, A. Woehr, K. L. Kratz, B. Pfeiffer, and W. B. Walters, *Phys. Rev. Lett.* **81**, 3100 (1998).
- [11] I. Stefanescu *et al.*, *Phys. Rev. Lett.* **100**, 112502 (2008).
- [12] K. Sieja and F. Nowacki, *Phys. Rev. C* **81**, 061303(R) (2010).
- [13] J. Van de Walle *et al.*, *Phys. Rev. Lett.* **99**, 142501 (2007).
- [14] Z. Y. Xu *et al.*, *Phys. Rev. Lett.* **113**, 032505 (2014).
- [15] X. F. Yang *et al.*, *Phys. Rev. Lett.* **116**, 182502 (2016); **116**, 219901(E) (2016).
- [16] R. Orlandi *et al.*, *Phys. Lett. B* **740**, 298 (2015).
- [17] A. Gottardo *et al.*, *Phys. Rev. Lett.* **116**, 182501 (2016).
- [18] M. Mukherjee *et al.*, *Eur. Phys. J. A* **35**, 1 (2008).
- [19] S. Kreim *et al.*, *Nucl. Instrum. Methods Phys. Res., Sect. B* **317**, 492 (2013).
- [20] K. Blaum, *Phys. Rep.* **425**, 1 (2006).
- [21] E. Kugler, *Hyperfine Interact.* **129**, 23 (2000).
- [22] P. A. Hausladen *et al.*, *Int. J. Mass Spectrom.* **251**, 119 (2006).
- [23] U. Köster, *Eur. Phys. J. A* **15**, 255 (2002).
- [24] V. N. Fedosseev *et al.*, *Rev. Sci. Instrum.* **83**, 02A903 (2012).
- [25] F. Herfurth *et al.*, *Nucl. Instrum. Methods Phys. Res., Sect. A* **469**, 254 (2001).
- [26] R. N. Wolf *et al.*, *Nucl. Instrum. Methods Phys. Res., Sect. A* **686**, 82 (2012).

- [27] R. N. Wolf *et al.*, *Int. J. Mass Spectrom.* **349–350**, 123 (2013).
- [28] F. Wienholtz *et al.*, *Int. J. Mass Spectrom.*, DOI: 10.1016/j.ijms.2017.07.016 (2017).
- [29] M. König, G. Bollen, H.-J. Kluge, T. Otto, and J. Szerypo, *Int. J. Mass Spectrom.* **142**, 95 (1995).
- [30] J. A. Winger, J. C. Hill, F. K. Wohn, E. K. Warburton, R. L. Gill, A. Piotrowski, R. B. Schuhmann, and D. S. Brenner, *Phys. Rev. C* **42**, 954 (1990).
- [31] M. Wang, G. Audi, F. G. Kondev, W. J. Huang, S. Naimi, and X. Xu, *Chin. Phys. C* **41**, 030003 (2017).
- [32] G. Audi, F. G. Kondev, M. Wang, W. J. Huang, and S. Naimi, *Chin. Phys. C* **41**, 030001 (2017).
- [33] L. Gaudefroy, A. Obertelli, S. Peru, N. Pillet, S. Hilaire, J. P. Delaroche, M. Girod, and J. Libert, *Phys. Rev. C* **80**, 064313 (2009).
- [34] M. Honma, T. Otsuka, T. Mizusaki, and M. Hjorth-Jensen, *Phys. Rev. C* **80**, 064323 (2009).
- [35] K. T. Flanagan *et al.*, *Phys. Rev. Lett.* **103**, 142501 (2009).
- [36] R. P. de Groote *et al.*, *Phys. Rev. C* **96**, 041302(R) (2017).
- [37] L. Olivier *et al.*, preceding Letter, *Phys. Rev. Lett.* **119**, 192501 (2017).
- [38] M. Bender, G. F. Bertsch, and P. H. Heenen, *Phys. Rev. C* **78**, 054312 (2008).
- [39] R. N. Wolf *et al.*, *Phys. Rev. Lett.* **110**, 041101 (2013).
- [40] D. Atanasov *et al.*, *Phys. Rev. Lett.* **115**, 232501 (2015).